Journal of Modern Physics, 2026, 17(8), 970-996
https://www.scirp.org/journal/jmp
ISSN Online: 2153-120X
ISSN Print: 2153-1196

How the Non-Axisymmetric Shape of the Milky Way Could Explain the Rotation Curve Flatness without Dark Matter

Bertrand Monteagle

21 Allée de la ferme, Issy Les Moulineaux, France
Email: Bertrand-m@hotmail.com

How to cite this paper: Monteagle, B. (2026) How the Non-Axisymmetric Shape of the Milky Way Could Explain the Rotation Curve Flatness without Dark Matter. *Journal of Modern Physics*, **17**, 970-996.
https://doi.org/10.4236/jmp.2026.178044

Received: June 16, 2026
Accepted: August 25, 2026
Published: August 28, 2026

Abstract

Instead of considering our Galaxy as a disc with a density directly dependent on the distance from the center of the Galaxy, the objective of this study is to propose a new method that will rely on a N-body simulation and a non-axisymmetric and fully baryonic mass model of our Galaxy. There are a lot of existing N-body simulations of our Galaxy about kinematics, as, for example, [1]. This is the first N-body simulation that allows to retrieve the rotation curves of the Milky Way, to retrieve the rotational speeds with a static model. This approach allows us to see the contribution of each arm to the rest of the Galaxy and to understand the flatness of the rotational curves between 10 and 15 kpc from the center of our Galaxy: the inner arm helps to accelerate the rotational motion, as the outer arm will decelerate it, but always lower than the acceleration brought by the inner arm.

Keywords

Milky Way, N-Body Simulation, Spiral Galaxy, Dark Matter

1. Introduction

We estimate there are around 2000 billion galaxies in the Universe [2]. Most of them are "spiral galaxies" [3]: a "flat" disc with a luminous center, named "Bulge", and several spiral arms (from 2 to 6 generally). Other kinds of galaxies exist in the Universe, with simpler shapes: elliptical galaxies, spherical galaxies, dwarf galaxies, …

Thanks to the study of rotation curves of the spiral galaxies, Vera Rubin, in 1978 [4], takes up the theory of Dark Matter to explain why the rotational speed remains constant outside the Bulge of our Galaxy (and not decreasing, as baryonic matter model predicted).

Vera Rubin used an axisymmetric "disc" type model, meaning that there is no variation in mass density along the tangential axis, only along the radial axis. This "axisymmetric disc model" has since been used by all the Dark Matter model studies (for example, Jiao in 2023 [5]).

Other studies based on our Galaxy's rotation curve (RC) have imagined other explanations for the "flat RC dilemma", with modified Newton's law for very low acceleration (near $10^{-10}\cdot\text{ms}^{-2}$): the MOND theory ([6]-[8]).

Some studies also used a modified mass distribution inside our Galaxy mixed with MOND ([9]-[13]), or even an idea of having a "Servomechanism" inside our Galaxy [14].

Recently, one article has stated that last Gaia Data coupled with the study of RC shows that MOND theory no longer works and Dark Matter existence is therefore confirmed [15].

But in the Dark Matter (DM) model, DM appears to be located mostly in spiral galaxies, and located specifically in the "spiral area" of the galaxies (outside the bulge). For example, in the Milky Way Bulge, less than 20% of the mass comes from DM, when 75% of the spiral area mass is DM, following [16].

From this starting point, one idea could be investigated: maybe the models we use for spiral galaxies (in order to estimate their masses) are not accurate enough. The spiral galaxies are flat disc-shaped, so all the existing models consider the spiral galaxies as being a flat disc, without considering their arms' shape.

This article's purpose is to use a more refined model of our Galaxy (with the spiral arms) and see the impacts on the rotational curve (and the mass estimation of our Galaxy).

2. Astrophysical Model

2.1. Overall View of the Milky Way

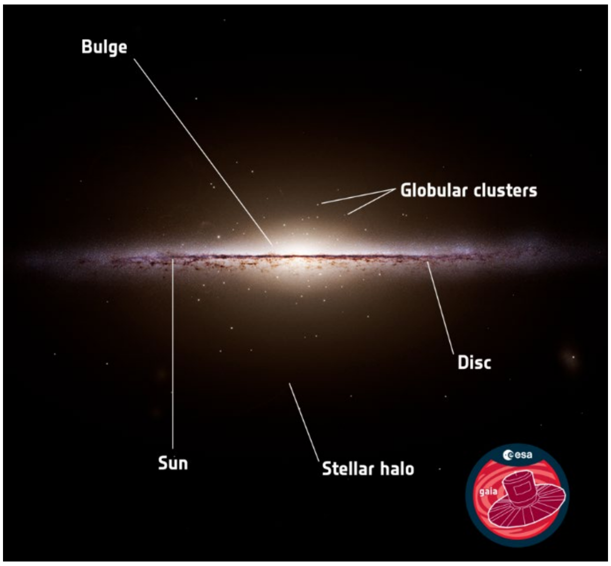

Figure 1. Profile view of our Galaxy (ESA image).

Our Galaxy, like most spiral galaxies, is composed of a bulge (highest stellar density, at the central part), the spirals that are mostly included in the same plane with a higher stellar density when we approach this plane (thin and dense disc) and less dense thick disc surrounding it. Moreover, the whole is included in an even lower stellar density sphere or halo shown in **Figure 1**.

We can clearly see in **Figure 1** the plane of symmetry of our Galaxy ($z = 0$).

If we were able to see our Galaxy from the outside, we could see the spiral shape of it on a face view, as shown in **Figure 2**.

Figure 2. Face view of our Galaxy (ESA image).

Our Galaxy is composed of several arms, linked to an Inner Ring, itself surrounding a bar-shaped Bulge at the center.

Our Sun is located at approx. 8.2 kpc from the center of the Galaxy [17] and can be considered as part of the symmetric plane of the Galaxy (it is lying 25 pc above the galactic plane [18]). Our Sun mass, $M_\odot$, is estimated to 1.99×10^{30} kg [19].

Also, our Galaxy turns clockwise (for **Figure 2**) in a very regular move: we estimate the galactic period of the Sun to be equal to approx. 240 million years [20], so our Galaxy has already completed dozens of turns since its creation.

Although there are vertical motion and an asymmetric drift slightly impacting the rotation curve [21], we will assume in this paper that the rotational motion is being fully planar (in the $z = 0$ plane of our Galaxy).

We will, as a main approx. consider that the Milky Way is a disc of 15 kpc radius and 2 kpc height and we will neglect the mass outside this disk for the study of the rotational motion of our Galaxy (the mass for 15 kpc < r < 26.5 kpc is estimated under $25 \times 10^9\ M_\odot$, when the mass for r < 15 kpc is estimated to $95.9 \times 10^9\ M_\odot$, see detailed explanations at the end of §2.4).

2.2. Dark Matter Model Disadvantages

DM "disc" models are often using linear relation between mass and radius to determine the mass of our Galaxy represented as a disc of radius r. For example, this equation, used in [22] and [5], is directly coming from Newton's law:

$$M(r) = \frac{V^2(r) * r}{G} \quad (1)$$

$M(r)$ being the mass for the disc of radius r;

$V(r)$ the circular speed at radius r;

G the gravitational constant.

This method has a lot of disadvantages. First, when the circular speed curve is flat (this is the case for Milky Way for 7 kpc < r < 15 kpc), the mass gradient $\frac{\mathrm{d}M}{\mathrm{d}r}$ is constant. It means that the mass grows linearly with the radius inside our Galaxy, up to immense radius values.

This unbalanced distribution is clearly not optimal and appears to be illogical after billions of years of circular motion of our Galaxy.

Also, it means, for the DM disc model, that the Mass gradient $\frac{\mathrm{d}M}{\mathrm{d}r}$ will drop abruptly for r > 20 kpc (when squared circular velocity drops far faster than r increases) and even become negative.

We expect a mass gradient to be decreasing slightly starting the moment when circular velocity is decreasing, and this is not the case with this model.

If you consider the mass distribution as only dependent on squared circular speed and radius (as shown Equation (1)), it means that when the circular speed drops, mass will also decrease.

For example, with this equation, if we consider that the circular speed is equal to 197.56 km·s^{-1} at r = 21.5 kpc, then 175.68 km·s^{-1} at r = 26.5 kpc (following [5] data), it means that:

$$M_{(r=21.5\,\text{kpc})} = \frac{1}{G} * 197560^2 * 21.5\ \text{kpc} = 195.0 * 10^9\ \mathrm{M}_\odot$$

$$M_{(r=26.5\,\text{kpc})} = \frac{1}{G} * 175680^2 * 26.5\ \text{kpc} = 190.0 \times 10^9\ \mathrm{M}_\odot$$

Following this model and calculation method, the mass decreases when volume increases.

2.3. 2D Modeling of Our Galaxy with a Reference Image

As explained at the end of §2.1, we will consider the rotational motion of our Galaxy as being fully planar.

It means that our model will be a 2d-model located inside the symmetry plane of our Galaxy, representing the volume masses of our Galaxy with bodies and allocated masses.

To do this, we needed the most accurate face view of our Galaxy, based on Gaia DR2. In 2019, for the first time, Khoperskov [23] provided evidence (see **Figure 3**) of the imprint left by spiral arms and resonances in the stellar densities not relying on a specific tracer, through enhancing the signatures left by these asymmetries, using coordinate space densities and radial velocity distributions.

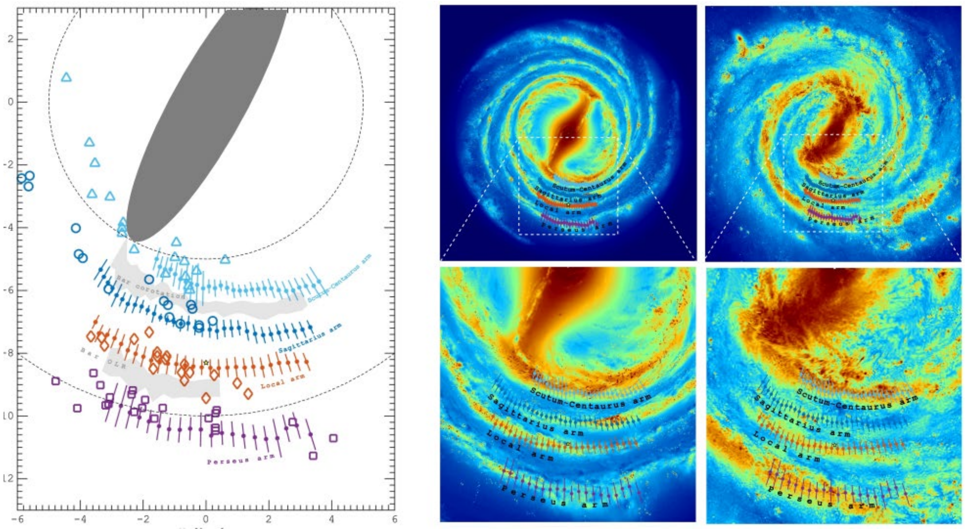

Figure 3. Milky Way spiral arms and bar resonances revealed by Gaia DR2. Based spiral arms shown by symbols with error bars (Khoperskov, 2019).

So, for the spiral and Inner Ring area, we decided to locate all the bodies of our model on the local center of gravity lines, *i.e.*, the arms axis (dotted lines below, **Figure 4**, *Milky Way Galaxy rendering by Robert Hurt and Nick Risinger* [23]).

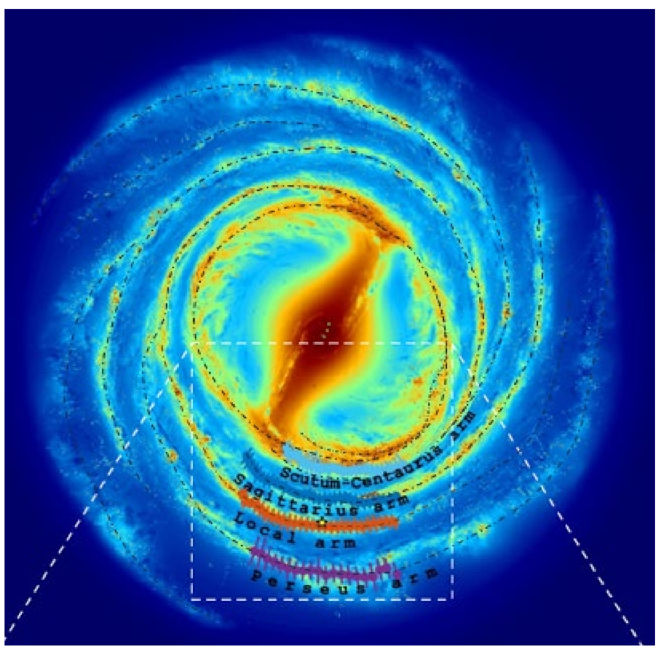

Figure 4. Location of local centers of gravity (Khoperskov, 2019).

Our model has 3324 bodies, distributed equidistantly, represented hereafter in **Figure 5**.

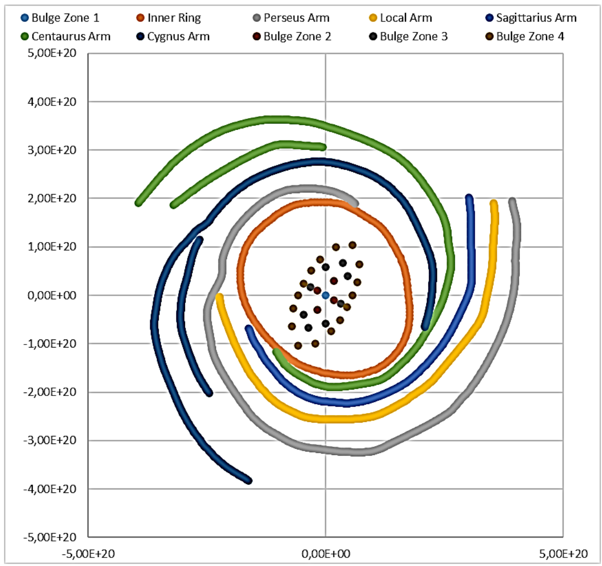

Figure 5. Inner Ring, Bulge and arms bodies (distances are in m).

We then need to allocate masses to each of those bodies.

2.4. Disc Baryonic Mass Distribution

In this article, we will not consider Dark Matter mass (or consider it as negligible).

We will compare our simulation data with a "DM + Baryonic" mass model (inspired by [5]) and a "Stellar + Gas" mass model (inspired by [24]).

For the "DM + Baryonic" mass model, as in [5], we choose a power-law with a power of $\alpha = -2.25$:

$$\rho_{disc} = \rho_0 * \left(\frac{1}{1+r}\right)^{2.25} \tag{2}$$

where r is the distance to the galactic center and ρ_0, the surface mass density at the galactic center (at $r = 0$), here equal to 41×10^9 M⊙ kpc^{-2} (following the value used by Miyamoto [25]).

For the "Stellar + Gas" mass model, we take as a reference the Surface density as a function of radius as measured by SEGUE G-dwarf samples and consider the gas mass, with an additional Surface Density (SD) of 13 M⊙ pc^{-2} (0.013×10^9 M⊙ kpc^{-2}) for all $r < 15$ kpc, following [24].

After several iterations (method explained in §2.9), we arrived at a surface density profile (the horizontal lines in **Figure 6**) slightly different from the "Stellar + Gas" mass model (red left curve in **Figure 6**), with areas having a growth factor linked to the arm's width (see explanations in **Appendix 1**). The simulation surface density profile is yet always lower than the DM + Baryonic surface density profile (yellow right curve in **Figure 6**).

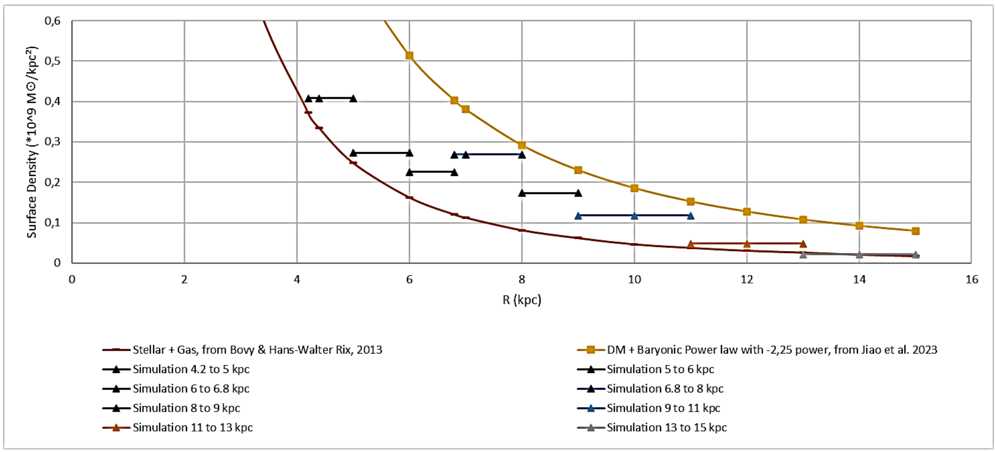

Figure 6. Surface Density (SD) simulation data Versus "Stellar + Gas" and "DM + Baryonic" models.

Hereafter in Table 1 is summarized the mass distribution in the Milky Way for r between 4.2 and 15 kpc (following surface density profile from Figure 6).

Table 1. Stellar & Gas mass distribution outside the Bulge & Inner Ring.

Mass (*10^9 M$_\odot$)	<6.8 kpc	6.8 kpc < r < 8 kpc	8 kpc < r < 9 kpc	9 kpc < r < 11 kpc	11 kpc < r < 13 kpc	13 kpc < r < 15 kpc	TOTAL
Perseus	0.3	**4.48**	1.76	1.78	2.27	0.71	11.36
Local		2.42	2.24	1.49	0.49		6.64
Sagittarius	1.94	1.58	0.83	1.62	0.44		6.42
Centaurus	**2.86**	3.26	1.53	**5.8**	**2.35**	**2.51**	**18.31**
Cygnus		3.25	**2.9**	4.18	1.68	0.54	12.55
TOTAL	5.1	**14.99**	9.26	14.87	7.23	3.76	**55.28**

The total dynamical mass M_{total} of our model is then equal to:

$$M_{Total} = M_{Bulge} + M_{InnerRing} + M_{Spiral} = 19.6 + 21 + 55.28 = 95.88 \times 10^9\ \mathrm{M}_\odot$$

M_{Bulge} is given in §2.5 while $M_{InnerRing}$ is given in §2.6 and M_{Spiral} in §2.7.

The Milky Way mass for $r > 15$ kpc is not above 25 × 10^9 M$_\odot$, following our power-law (calculation given in **Appendix 3**).

2.5. Bulge Baryonic Mass Distribution Cartography and Bodies' Location

The Bulge has a "bar-shaped" aspect [26] that will increase gravitational forces along that bar's axis (asymmetrical shape impact).

We assume that Bulge mass M_{Bulge} is equal to 19.6 billion M$_\odot$, following Bulge E values used in [5].

From Portail [16], we can also observe a clear gap between surface density profile following the minor axis and the one following the major axis of the bulge.

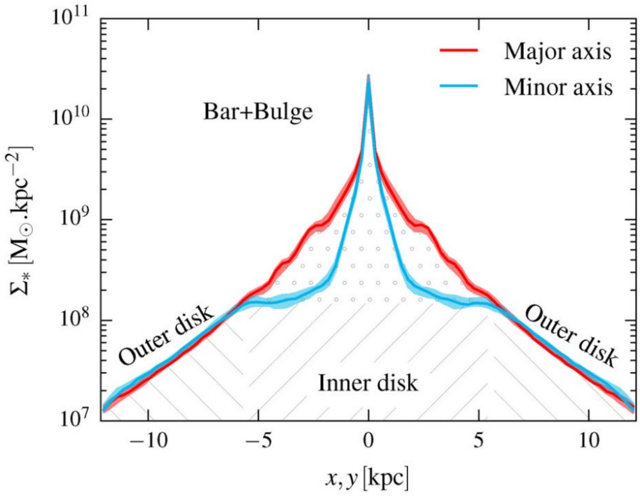

Figure 7. Surface Density (SD) profile of the Bulge, following minor and major axes (Portail *et al.*, 2017) [16].

We will consider the mass distribution of **Figure 7** for the Bulge meshing cartography.

We will consider 4 different zones as described below in **Figure 8**.

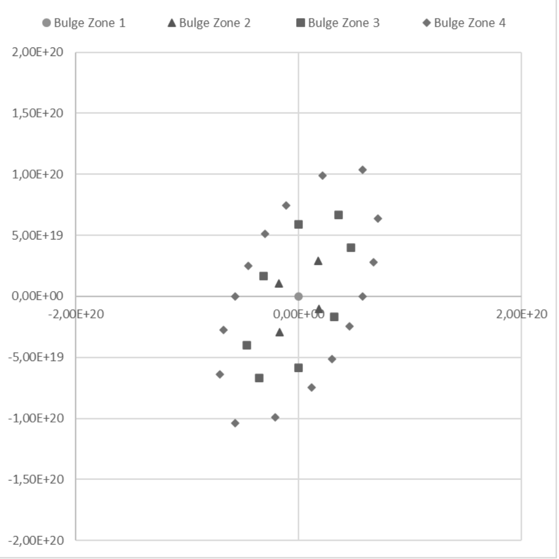

Figure 8. Bulge bodies (distances are in m).

Zone 1, with a "major axis" diameter of 1.15 kpc and a "minor axis" diameter of 0.66 kpc, will be represented by one body, at the center of the Galaxy with a mass equal to 3.2×10^9 M⊙ (SD = 5×10^9 M⊙/kpc²).

Surrounding Zone 1 is Zone 2 with a "major axis" diameter of 3.63 kpc and a "minor axis" diameter of 1.87 kpc, will be represented by 4 bodies, each with a 1.25 × 10^9 M⊙ mass (SD = 1 × 10^9 M⊙/kpc^2).

Surrounding Zone 2 is Zone 3 with a "major axis" diameter of 6.71 kpc and a "minor axis" diameter of 2.97 kpc, will be represented by 8 bodies, each with a 0.5375 × 10^9 M⊙ mass (SD = 0.4 × 10^9 M⊙/kpc^2).

Surrounding Zone 3 is Zone 4 with a "major axis" diameter of 11.66 kpc and a "minor axis" diameter of 5.06 kpc, will be represented by 16 bodies, each with a 0.44375 × 10^9 M⊙ mass (SD = 0.25 × 10^9 M⊙/kpc^2).

The total mass for the Bulge is then:

$M_{Bulge} = M_{Zone1} + M_{Zone2} + M_{Zone3} + M_{Zone4} = 3.2 + 5 + 4.3 + 7.1 = 19.6 \times 10^9\ M_\odot$, as expected.

2.6. Inner Ring Mass Distribution Cartography and Bodies' Location

We will consider a mass of the Inner Ring $M_{InnerRing}$ equal to 21 × 10^9 M⊙ (calculation explained in **Appendix 2**).

We place the bodies equidistantly on the center of gravity line representing the Inner Ring (thanks to GMesh tool), as shown in Figure 9.

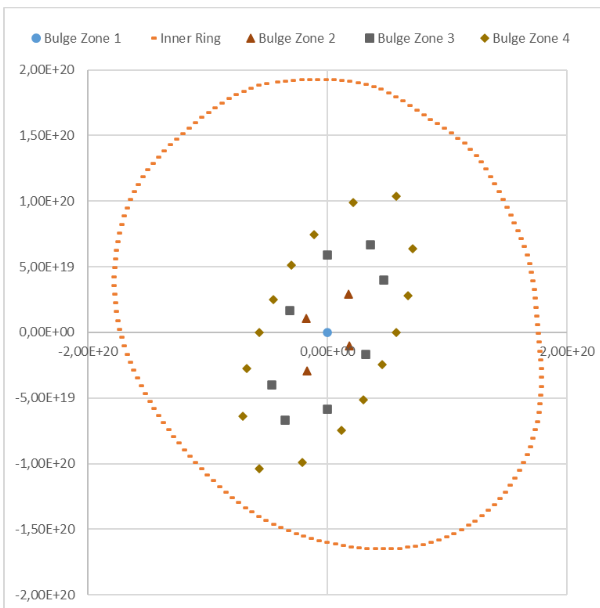

Figure 9. Inner ring and bulge bodies (distances are in m).

Inner Ring is represented by 167 bodies, with 0.22 kpc between the bodies.

2.7. Arms Mass Distribution Cartography and Location of the Bodies

For the arms, we will take a more refined value of 0.07 kpc for the inter-body distance. This is far above the 0.0013 kpc median distance between stars in our Galaxy and far under the 1 kpc minimal distance between arms.

The total mass for the arms M_{Spiral} will be 55.28×10^9 M☉ as explained in **Table 1**. The allocated mass per body follows strictly the distribution per arm and per area described in **Table 1**.

A single body represents roughly all the mass around including stars systems, rogue planets, dust, gas, … (in a box delimited by the half-distance with others nodes of the arm.)

2.8. Global Hypotheses and Equations Used in the N-Body Simulation

Our main hypothesis is to consider that our Galaxy is not axisymmetric.

While studies already exist regarding the asymmetric distribution of gas in our Galaxy and its impact [27], this study extends this concept to all baryonic matter.

Even if the variations of stellar density are low (See **Figure 10** from Khoperskov [23]), we can observe many non-axisymmetric areas in our Galaxy.

We can observe that there are many "junction areas" (between arms and between arms and the Inner Ring), and even the arms do not have all the same shape or length.

As the gravitational forces are mostly responsible for the global rotational movement of our Galaxy, we can imagine that in some areas, the circular movement will be almost uniform, while in other areas it will not.

For the "spiral area" (outside the Inner Ring), we will consider the rotational movement as being uniform (radial speed being negligible), but inside the "junction areas" we will consider that the radial speed is too high to only consider the tangential movement (see **Figure 11**, based on *Milky Way Galaxy rendering by Robert Hurt and Nick Risinger* [23]).

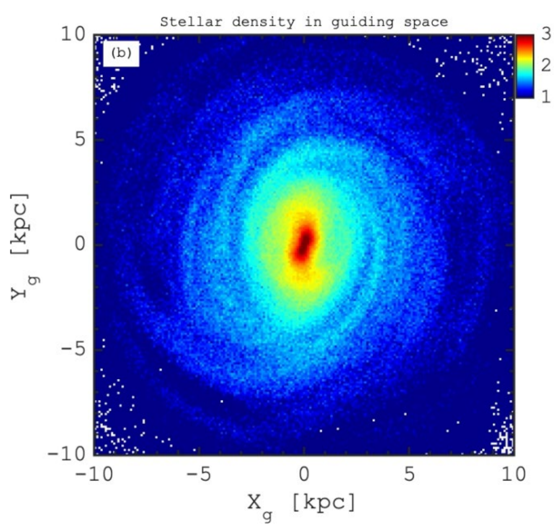

Figure 10. Stellar density in the Milky Way (Khoperskov, 2019).

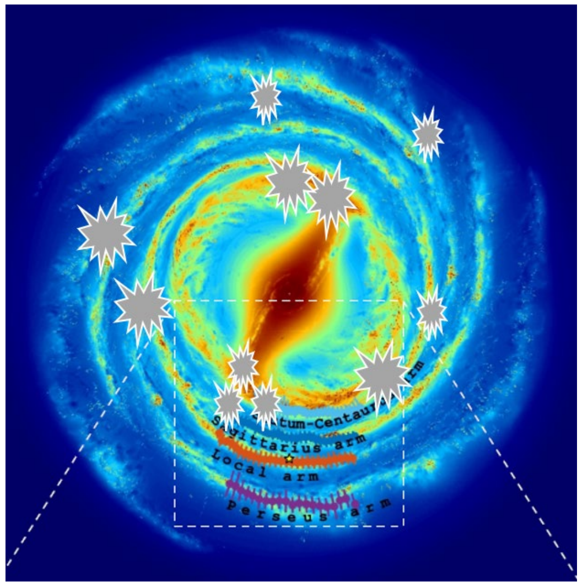

Figure 11. Areas without uniform circular motion (Khoperskov, 2019).

We will exclude those areas in our model post-processing.

We will only consider the areas in the spiral zone, where the inner and outer arms are not too close (in order to avoid gravitational impact on radial velocity and rotational motion).

Also, we will exclude the nearby bodies (assuming the average distance between arms is equal to 2 kpc, we will exclude the contribution of all bodies closer than 1 kpc).

This is only to avoid having data "fog" and to better see the velocity trend on the curves, as shown in **Figure 12**.

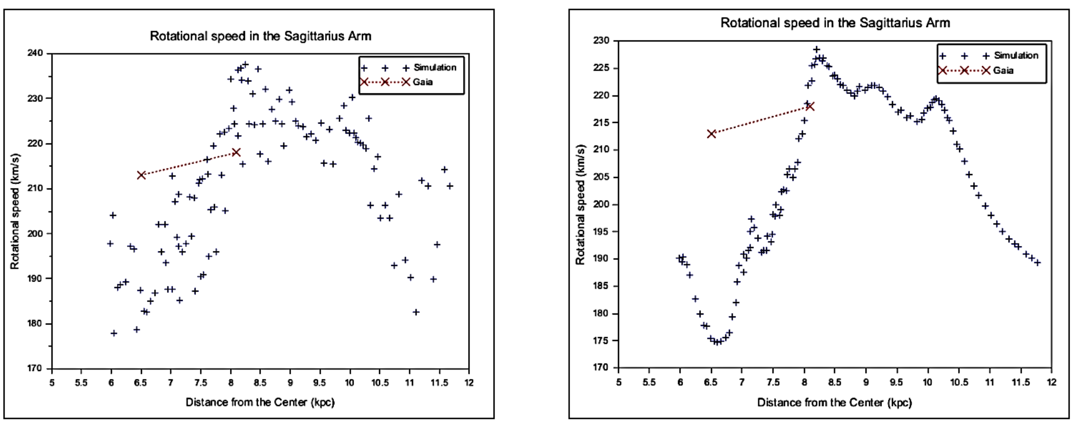

Rotation curves with nearby bodies (V4 results / those results are not final results)

Rotation curves without nearby bodies (V4 results / those results are not final results)

Figure 12. Results with nearby bodies (left side) and without nearby bodies (right side).

For the uniform circular motion outside those areas, we will use the equation of uniform circular motion:

$$a_r = \frac{v_{rot}^2}{r} \quad (3)$$

a_r being the radial acceleration (in m·s^{-2});

v_{rot} the rotational speed (in m·s^{-2});

r the radius (in m).

At each body of our model (with position $I\,[x(i);\ y(i)]$ and mass $m(i)$), we will calculate the contribution to radial acceleration given by each other body (with position $J\,[x(j);\ y(j)]$ and mass $m(j)$) by

$$a_r\left(\text{on } I \text{ from } J\right) = \frac{G * m(j)}{\sqrt{\left(\left(x(i)-x(j)\right)^2 + \left(y(i)-y(j)\right)^2\right)^2}} * \cos\left(\widehat{OIJ}\right) \quad (4)$$

G being the gravitational constant, equal to 6.7×10^{-11} m^3·kg^{-1}·s^{-2}.

Positions of $I\,[x(i);\ y(i)]$ and $J\,[x(j);\ y(j)]$ are given relatively to the origin point $O\,[0;\ 0]$, in m.

$m(j)$ the mass of the point J, in kg.

$\widehat{OIJ}$ the angle between IO and IJ (allowing us to know the acceleration projected onto radial axis).

By summing the radial accelerations contributed by each distributed element, we can thus find total radial acceleration at point I ("N" being the number of bodies in the model):

$$a_{r\ Total}\left(I\right) = \sum_{j=0}^{j=i-1} a_r\left(\text{on } I \text{ from } J\right) + \sum_{j=i+1}^{j=N} a_r\left(\text{on } I \text{ from } J\right) \quad (5)$$

Following Equation (3), the associated speed of rotation is:

$$v_{rot} = \sqrt{a_r * r} \quad (6)$$

Then,

$$v_{rot}\left(I\right) = \sqrt{a_{r\ Total}\left(I\right) * \sqrt{x(i)^2 + y(i)^2}} \quad (7)$$

The iterative calculations will allow us to reach the results obtained by Gaia data (rotation speeds of stars). Gaia data are given at $z = 0$ plane with median values of rotational speeds.

The simulation results will also be median values for an area equivalent to a square with the size of inter bodies distance (0.07 kpc).

As we can see for the Local Arm, the arm's stellar density is maximum for a width that can be above the inter bodies distance, so we will have to apply a growth factor on arms with a spread stellar density (see **Appendix 1**).

2.9. How to Iterate on the N-Body Simulation Thanks to Gaia Data

The iteration calculations principle is simple: we will target the desired results and try to reach them by iterating on our model (bodies locations or mass distribution).

Hereafter, in Table 2, are the rotational speed median values for 6 kpc < r < 15 kpc area coming from Gaia DR3 summarized in [5]:

Table 2. Milky Way Gaia DR3 measurements data.

Radius (in kpc)	Circular velocity (km·s^{-1})
6	212
7	215
8	218
9	220
10	222
11	222
12	223
13	223
14	222
15	220

Those data are then incorporated into our results graph, in order to see the gap between the obtained simulation results and the real data from Gaia DR3 (crossed lines in Figure 13).

2.10. Model Uncertainties

Gaia Data

Systematic uncertainties from Gaia data DR3 rotational speeds are limited, especially for $r < 15$ kpc area, as last studies on Milky Way Rotational Curve show gaps of less than 5% between studies [5].

Mass distribution models

We have also decided to choose a model for Bulge mass distribution, given by [5], which could have lot of uncertainties for $r < 4$ kpc, but the shape impact of the Bulge will decrease with $r > 4$ kpc (as the impact of the Bulge on the results, see §4.2).

For the Disc (including Inner Ring) surface density profile, we have used, as a basis, a power-law that contains all the baryonic components (Stellar, Gas and Dust). We estimate global uncertainties of ~10% in the overall mass estimation for the disc.

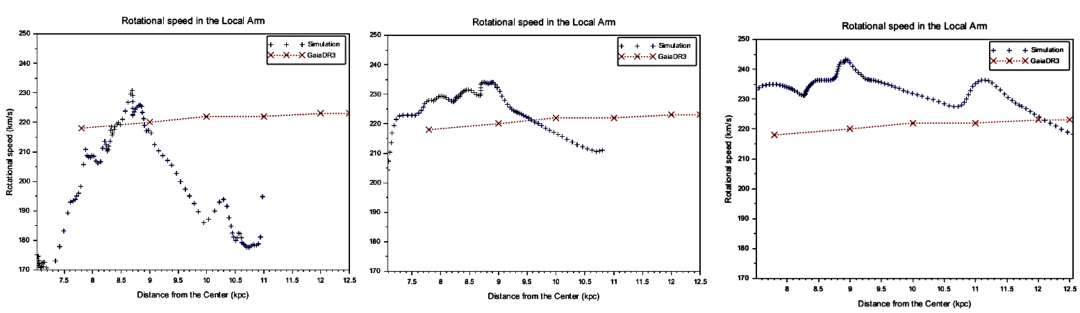

V1 V14 V27

Figure 13. Gaia Results incorporated in the simulation results for different iteration calculations.

Uniform circular motion

We consider the rotational motion as being sufficiently "slow" (one turn every 250 million years) to conduct a static study on rotational speed. This means we consider the object's location as static even while studying the velocities of those objects.

As we consider a 0.4 kpc = 1.23×10^{16} m approximation for distances, dividing the distance by an average rotational speed of 200,000 $m \cdot s^{-1}$ yields an average time of 6.15×10^{10} s, which is approx. 1950 years of motion without exceeding the distance uncertainties.

However, even with this good approach, the radial component of speed is never negligible (see §4.2) and could introduce an uncertainty in rotational speed comparable to the ratio between radial and rotational speeds (up to 20%).

2D model

We do not consider the vertical velocities (*i.e.*, along the z axis), nor the vertical locations of the Milky Way objects.

We also do not consider the vibrations or modal motion that impact the Milky Way motion.

Furthermore, we exclude from our model the dwarf galaxies or other star clusters (and more broadly, everything that is outside $|z| < 3$ kpc and $|r| < 15$ kpc). We consider their masses as being negligible and having no impact on the $|z| < 3$ kpc and $|r| < 15$ kpc disc.

This adds another < 5% uncertainty to the results.

A solution against uncertainties: iterative calculations

All those uncertainties combined could lead to an impact of approx. 30% on the rotational speeds.

Nevertheless, the iterative method helps us to converge to the level of uncertainties due to Gaia Data, because our calculations and iterations will be driven by that data.

Then, we can state that we have the uncertainty level of [5] study, *i.e.*, around 10%.

3. Scilab Model and Post-Processing

3.1. Presentation of Scilab

Scilab is a free and open-source platform that allows large-scale simulation.

This tool is a good solution for N-body simulation, as it allows coding without using declarative programming, and offers a large choice of post-processing graphics.

It is one of the most well-known alternatives to MATLAB tool.

3.2. Presentation of the Code

We divided the code files by areas (5 files for the 5 arms of our Galaxy: Local, Perseus, Centaurus, Sagittarius and Cygnus).

For all the files, we will first establish the constants (gravitational constant, masses, coordinates of the bodies …), as displayed exemplarily in Figure 14:

```
//constants
G=6.7*10^-11;//Gravitational constant (m3Kg-1s-2)

//masses (Kg)

m = [6.4E+39    2.5E+39 2.5E+39 2.5E+39 2.5E+39 1.075E+39    1.075E+39    1.075E+39    1.075E+39    1.075E+39    1.075E+39    1.075E+39    1.075E+39    8.
    4.75E+37    4.75E+37    4.75E+37    4.75E+37    4.75E+37    4.75E+37    4.75E+37    4.75E+37    4.75E+37    4.75E+37    4.75E+37    4.75E+37
    4.00E+37    4.00E+37    4.00E+37    4.00E+37    4.00E+37    4.00E+37    4.00E+37    4.00E+37    4.00E+37    4.00E+37    4.00E+37    4.00E+37
    1.85E+37    1.85E+37    1.85E+37    1.85E+37    1.85E+37    1.85E+37    1.85E+37    1.85E+37    1.85E+37    1.85E+37    1.85E+37    1.85E+37
    2.57E+37    2.57E+37    2.57E+37    2.57E+37    2.57E+37    2.57E+37    2.57E+37    2.57E+37    2.57E+37    2.57E+37    2.57E+37    2.57E+37
    4.07E+37    4.07E+37    4.07E+37    4.07E+37    4.07E+37    4.07E+37    4.07E+37    4.07E+37    4.07E+37    4.07E+37    4.07E+37    4.07E+37
    2.70E+37    2.70E+37    2.70E+37    2.70E+37    2.70E+37    2.70E+37    2.70E+37    2.70E+37    2.70E+37    2.70E+37    2.70E+37    2.70E+37
    4.06E+37    4.06E+37    4.06E+37    4.06E+37    4.06E+37    4.06E+37    4.06E+37    4.06E+37    4.06E+37    4.06E+37    4.06E+37    4.06E+37
    3.36E+37    3.36E+37    3.36E+37    3.36E+37    3.36E+37    3.36E+37    3.36E+37    3.36E+37    3.36E+37    3.36E+37    3.36E+37    3.36E+37
    4.81E+37    4.81E+37    4.81E+37    4.81E+37    4.81E+37    4.81E+37    4.81E+37    4.81E+37    4.81E+37    4.81E+37    4.81E+37    4.81E+37
    4.00E+37    4.00E+37    4.00E+37    4.00E+37    4.00E+37    4.00E+37    4.00E+37    4.00E+37    4.00E+37    4.00E+37    4.00E+37    4.00E+37
    1.97E+37    1.97E+37    1.97E+37    1.97E+37    1.97E+37    1.97E+37    1.97E+37    1.97E+37    1.97E+37    1.97E+37    1.97E+37    1.97E+37
    5.13E+37    5.13E+37    5.13E+37    5.13E+37    5.13E+37    5.13E+37    5.13E+37    5.13E+37    5.13E+37    5.13E+37    5.13E+37    5.13E+37
    4.80E+37    4.80E+37    4.80E+37    4.80E+37    4.80E+37    4.80E+37    4.80E+37    4.80E+37    4.80E+37    4.80E+37    4.80E+37    4.80E+37
    1.85E+37    1.85E+37    1.85E+37    1.85E+37    1.85E+37    1.85E+37    1.85E+37    1.85E+37    1.85E+37    1.85E+37    1.85E+37    1.85E+37
    1.97E+37    1.97E+37    1.97E+37    1.97E+37    1.97E+37    1.97E+37    1.97E+37    1.97E+37    1.97E+37    1.97E+37    1.97E+37    1.97E+37
    3.50E+37    3.50E+37    3.50E+37    3.50E+37    3.50E+37    3.50E+37    3.50E+37    3.50E+37    3.50E+37    3.50E+37    3.50E+37    3.50E+37

//coordinates (m)

x=[0    1.78815E+19 -1.78815E+19    1.73047E+19 -1.73047E+19    -3.5763E+19 3.5763E+19  3.17252E+19 -3.17252E+19    0   0   -4.67226E+19    4.6722
-1.22641E+20    -1.17312E+20    -1.11918E+20    -1.0647E+20 -1.0095E+20 -9.53378E+19    -8.96153E+19    -8.37646E+19    -7.77708E+19    -7.16233E+
-2.13145E+20    -2.13875E+20    -2.14576E+20    -2.15242E+20    -2.15858E+20    -2.16387E+20    -2.16827E+20    -2.17183E+20    -2.1746E+20 -2.176
    -1.65888E+20    -1.64503E+20    -1.63105E+20    -1.61695E+20    -1.60272E+20    -1.58835E+20    -1.57382E+20    -1.55914E+20    -1.54428E+20
    1.99521E+20 2.01526E+20 2.03528E+20 2.05527E+20 2.07524E+20 2.09518E+20 2.11508E+20 2.13494E+20 2.15475E+20 2.17453E+20 2.19429E+20 2.21402E+2
    4.02125E+20 4.02368E+20 4.02604E+20 4.02829E+20 4.03039E+20 4.03233E+20 4.03405E+20 4.03553E+20 4.03673E+20 4.03762E+20 4.03816E+20 4.03833E+2
    -7.58768E+19    -7.38546E+19    -7.18293E+19    -6.98025E+19    -6.77762E+19    -6.57499E+19    -6.37213E+19    -6.16874E+19    -5.96453E+19
    2.95728E+20 2.97111E+20 2.985E+20   2.99892E+20 3.01286E+20 3.02681E+20 3.04075E+20 3.05467E+20 3.06855E+20 3.08236E+20 3.0961E+20  3.10975E+2
```

Figure 14. Constants used in Scilab files.

Then we declare the radial acceleration, rotational speed, and distance matrix (initially set to 0). We then launch a double loop: for all the points located in the arm (for example, hereafter the Local Arm in Figure 15), we will calculate the contribution to radial acceleration given by each of the other bodies in the model:

We can also see in Figure 15 the calculation of the cosine that retrieves the radial acceleration for all bodies.

```
Acceltotal = [0,0,0,0,0,0,0,0,0,0,0,0,0,0,0,0,0,0,0,0,0,0,0,0,0,0,0,0,0,0,0,0,0,0,0,0,0,0

Speed = [0,0,0,0,0,0,0,0,0,0,0,0,0,0,0,0,0,0,0,0,0,0,0,0,0,0,0,0,0,0,0,0,0,0,0,0,0,0,0,

Distance = [0,0,0,0,0,0,0,0,0,0,0,0,0,0,0,0,0,0,0,0,0,0,0,0,0,0,0,0,0,0,0,0,0,0,0,0,0,0


d=0

//Local Arm loop

for i= 1020:3:1370
d=d+1
e=i-14
f=i+14

//Radial acceleration calculation (ms-2)
for j = 1:e
disp(j)

module = G*m(j) / (sqrt(((x(i)-x(j))^2+(y(i)-y(j))^2))^2;

//Cosine calculation for radial acceleration
DotProduct = x(i)*(x(i)-x(j))+y(i)*(y(i)-y(j))
Norm1 = sqrt((x(j)-x(i))^2+(y(j)-y(i))^2)
Norm2 = sqrt((x(i))^2+(y(i))^2)
Caussinus = DotProduct / (Norm1*Norm2)
module = module*Caussinus
Acceltotal(d) = Acceltotal(d) + module
end

for j = f:3324
disp(j)

module = G*m(j) / (sqrt(((x(i)-x(j))^2+(y(i)-y(j))^2))^2;
```

Declaration of Acceleration, Speed and distance matrices

Loop on all the nodes of the arm

We excludes the nearby nodes

First part of the calculations on each node until the node of the arm

Second part of the calculations on each node from the node of the arm until last node of the model

Figure 15. Calculations in Scilab files (Local Arm file).

4. Results

4.1. Rotational Speed

As shown in Figure 16, for all the arms, the Gaia observed circular speeds are reached, even if the curve allure is not matching everywhere (non-axisymmetric behavior explained in §4.2):

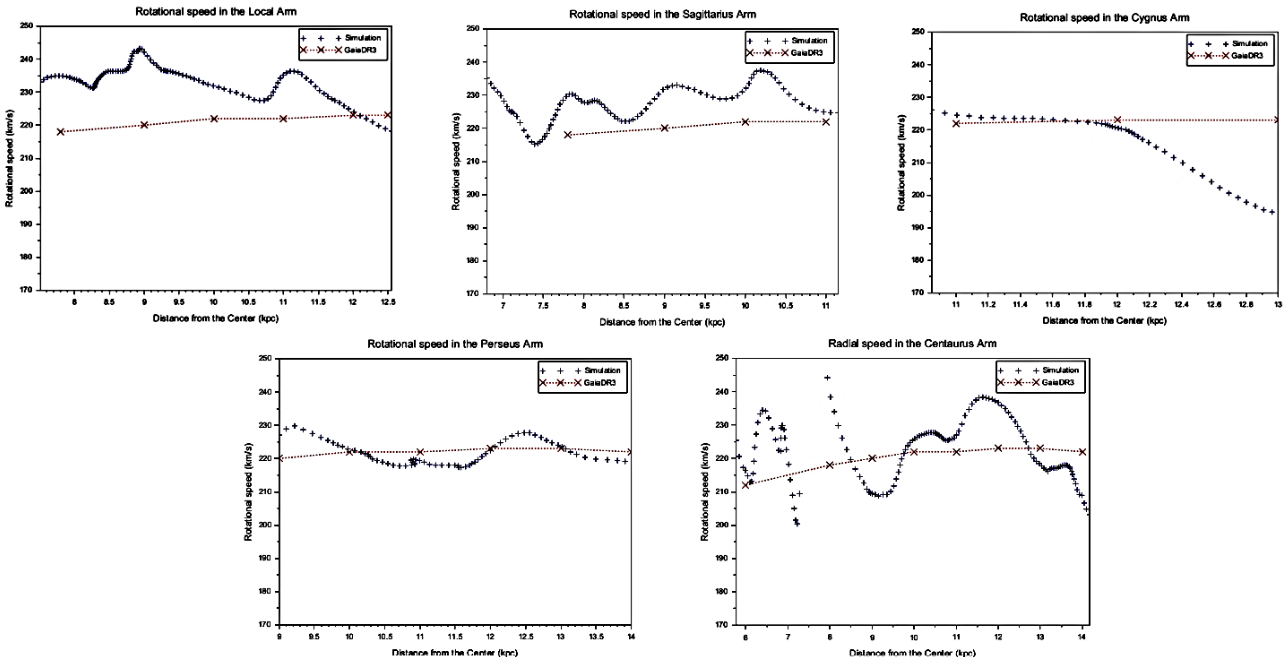

Figure 16. Milky Way circular velocities from N-body simulation.

Rotational speed with Axisymmetric model

By using Table 1 and Table 2 data and by using Equation (1), we obtain the results given in Table 3:

Table 3. Axisymmetric circular velocity with simulation data.

Radius (in kpc)	Radius (in m)	$M(r)$ model non axi (in kg)	Circular Velocity ($km \cdot s^{-1}$)
6,8	2,09848E+20	9,0943E+40	170,07
8	2,4688E+20	1,20773E+41	180,69
9	2,7774E+20	1,39201E+41	182,89
11	3,3946E+20	1,68792E+41	182,17
13	4,0118E+20	1,8318E+41	174,57
15	4,6290E+20	1,90662E+41	165,80

From Figure 17, we clearly see that the results are far lower with an axisymmetric model:

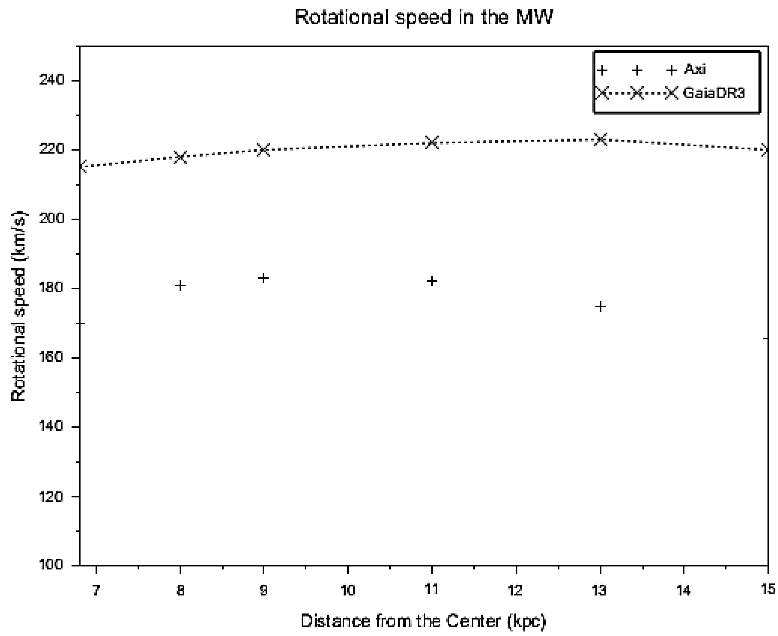

Figure 17. Milky Way Circular velocities from axisymmetric model with N-body simulation data.

With an axisymmetric model, we lose on average 20% on the circular velocity and need an additional 36% on global mass (following Equation (1)).

4.2. Contributions

In the "disc model" with Dark Matter, all the contributions on the radial acceleration are positive, *i.e.* all the parts of the Milky Way have a positive contribution to the rotational speed, and the total velocity is basically the sum of all the "partial velocities" (Sum of DM "Einasto" + Baryon or sum of Bulge + Disc + Dust + Gas = Total velocity, show in Figure 18 taken from [5]):

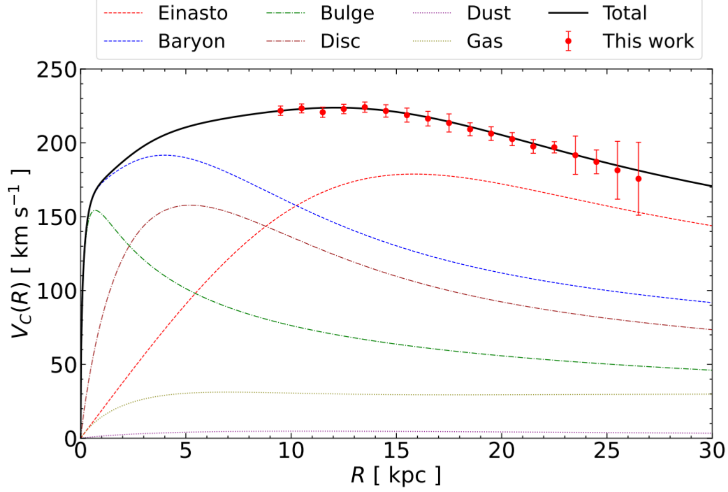

Figure 18. Milky Way circular velocities from Jiao *et al.* 2023 [5].

We can do exactly the same with our calculations, knowing that our bodies are numbered together per area. For example, in Figure 19 we show the bodies used for the Bulge (ID between 1 and 29).

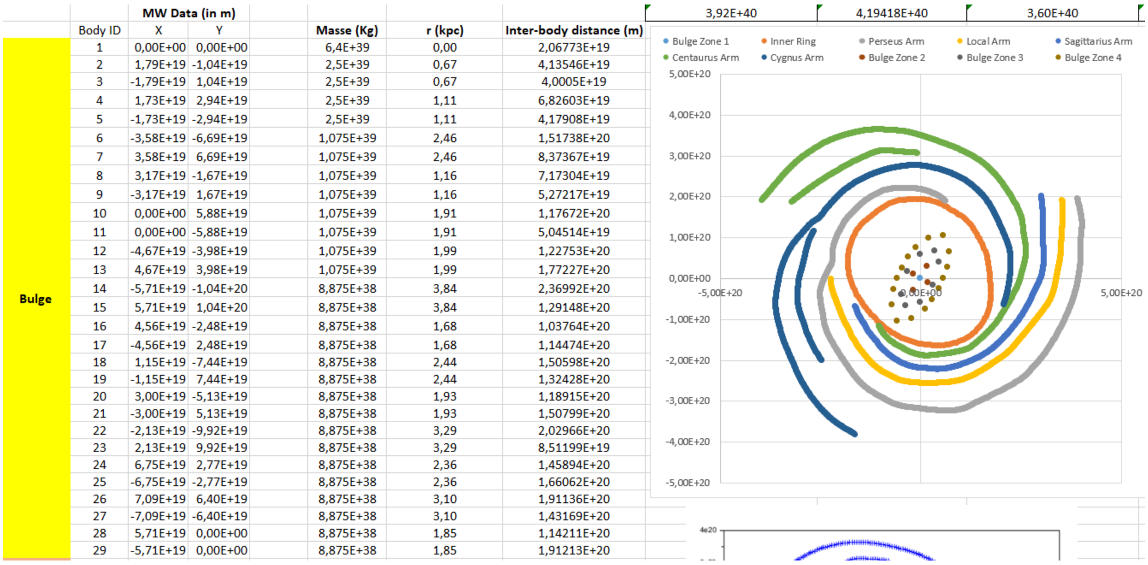

		MW Data (in m)		Masse (Kg)	r (kpc)	Inter-body distance (m)
	Body ID	X	Y			
Bulge	1	0,00E+00	0,00E+00	6,4E+39	0,00	2,06773E+19
	2	1,79E+19	-1,04E+19	2,5E+39	0,67	4,13546E+19
	3	-1,79E+19	1,04E+19	2,5E+39	0,67	4,0005E+19
	4	1,73E+19	2,94E+19	2,5E+39	1,11	6,82603E+19
	5	-1,73E+19	-2,94E+19	2,5E+39	1,11	4,17908E+19
	6	-3,58E+19	-6,69E+19	1,075E+39	2,46	1,51738E+20
	7	3,58E+19	6,69E+19	1,075E+39	2,46	8,37367E+19
	8	3,17E+19	-1,67E+19	1,075E+39	1,16	7,17304E+19
	9	-3,17E+19	1,67E+19	1,075E+39	1,16	5,27217E+19
	10	0,00E+00	5,88E+19	1,075E+39	1,91	1,17672E+20
	11	0,00E+00	-5,88E+19	1,075E+39	1,91	5,04514E+19
	12	-4,67E+19	-3,98E+19	1,075E+39	1,99	1,22753E+20
	13	4,67E+19	3,98E+19	1,075E+39	1,99	1,77227E+20
	14	-5,71E+19	-1,04E+20	8,875E+38	3,84	2,36992E+20
	15	5,71E+19	1,04E+20	8,875E+38	3,84	1,29148E+20
	16	4,56E+19	-2,48E+19	8,875E+38	1,68	1,03764E+20
	17	-4,56E+19	2,48E+19	8,875E+38	1,68	1,14474E+20
	18	1,15E+19	-7,44E+19	8,875E+38	2,44	1,50598E+20
	19	-1,15E+19	7,44E+19	8,875E+38	2,44	1,32428E+20
	20	3,00E+19	-5,13E+19	8,875E+38	1,93	1,18915E+20
	21	-3,00E+19	5,13E+19	8,875E+38	1,93	1,50799E+20
	22	-2,13E+19	-9,92E+19	8,875E+38	3,29	2,02966E+20
	23	2,13E+19	9,92E+19	8,875E+38	3,29	8,51199E+19
	24	6,75E+19	2,77E+19	8,875E+38	2,36	1,45894E+20
	25	-6,75E+19	-2,77E+19	8,875E+38	2,36	1,66062E+20
	26	7,09E+19	6,40E+19	8,875E+38	3,10	1,91136E+20
	27	-7,09E+19	-6,40E+19	8,875E+38	3,10	1,43169E+20
	28	5,71E+19	0,00E+00	8,875E+38	1,85	1,14211E+20
	29	-5,71E+19	0,00E+00	8,875E+38	1,85	1,91213E+20

Figure 19. Meshing file extract, Bulge bodies' ID.

In order to calculate the rotational speed of a specific arm, we will first plot the contribution due to Bulge and Inner Ring (+ curve), then plot the contribution due to Bulge + IR + Perseus + Local (o curve), then the contribution due to Bulge + IR + Perseus + Local + Sagittarius (*curve) then the same with Bulge + IR + Perseus + Local + Sagittarius + Centaurus (x curve) and finally adding Cygnus contribution to retrieve the total rot speed.

For example, for the Local Arm, the results are shown in Figure 20 (arrows are added to clarify the contributions).

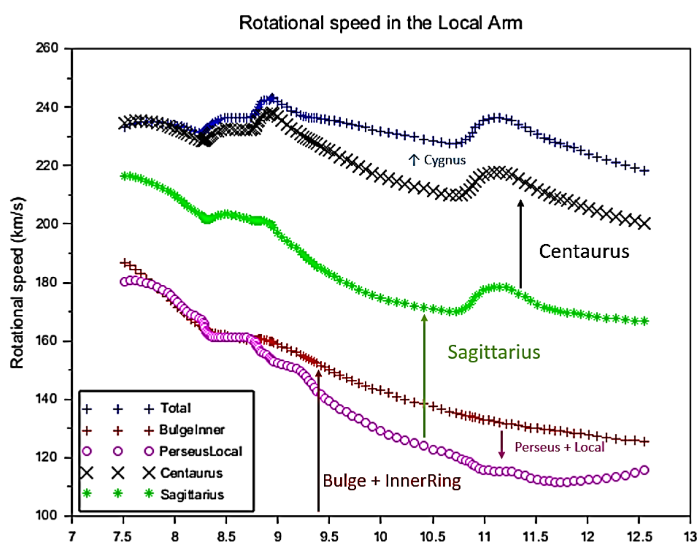

Figure 20. Local arm circular velocities.

We can see in Figure 20 that all the arms have a positive contribution to the Local Arm radial acceleration, except the Perseus Arm (the outer arm of the Local Arm), which globally decelerates the Local Arm.

In contrast, the Sagittarius Arm and the Centaurus Arm (which are the inner arms of the Local Arm) contribute significantly to radial acceleration and, consequently, circular velocity.

It is also interesting to note that in the case of the Local Arm, it is the Cygnus Arm that helps maintain the circular velocity for $r > 9$ kpc, because the "start" of the Cygnus Arm is located near this area (see Figure 21).

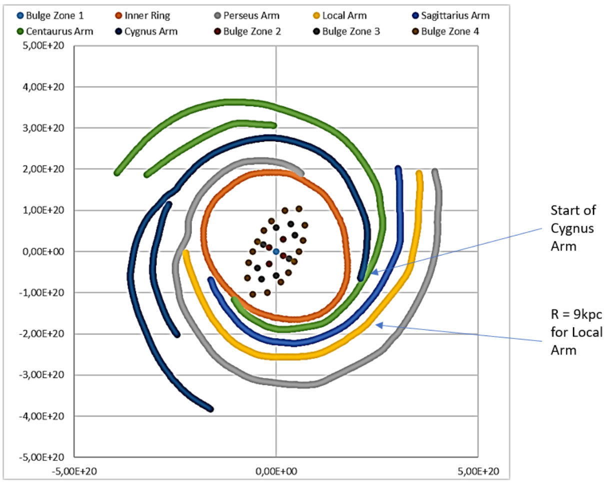

Figure 21. Cygnus and local arms location.

We also see a little "bump" in the Sagittarius contribution for $r \approx 11$ kpc, which is due to a rapprochement between the two arms in this area.

For the Perseus Arm, all arms will have a positive contribution to rotational speed, as shown in Figure 22, except for the $r < 9.5$ kpc area, where the Cygnus Arm has a small negative impact:

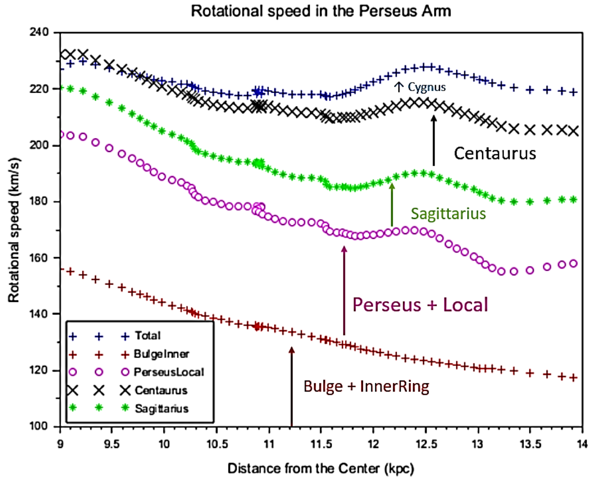

Figure 22. Perseus arm circular velocities.

This is also consistent with our model, as we can see in **Figure 23**: the Perseus Arm is the outer arm of all the other arms, except for the Cygnus Arm and for $r < 9.5$ kpc.

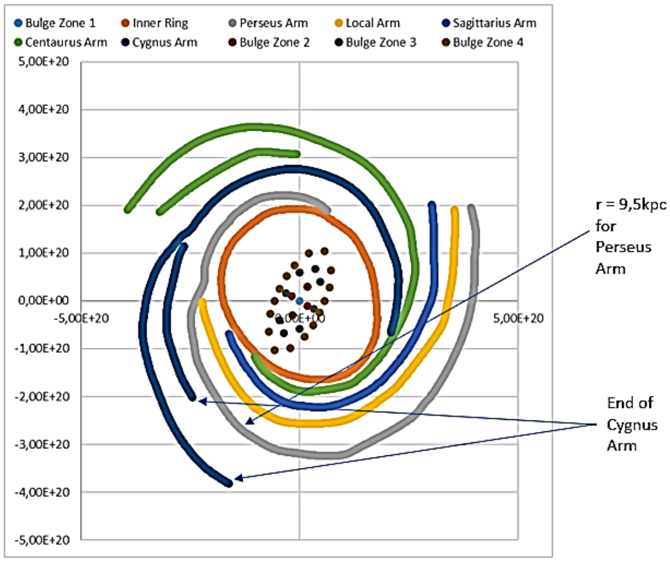

Figure 23. Cygnus and perseus arms location.

For the Sagittarius Arm, we see in **Figure 24** that Local and Perseus Arms have large negative impact (outer arm), whereas Centaurus gives an important contribution and Cygnus starts with a positive contribution for $r > 8.5$ kpc.

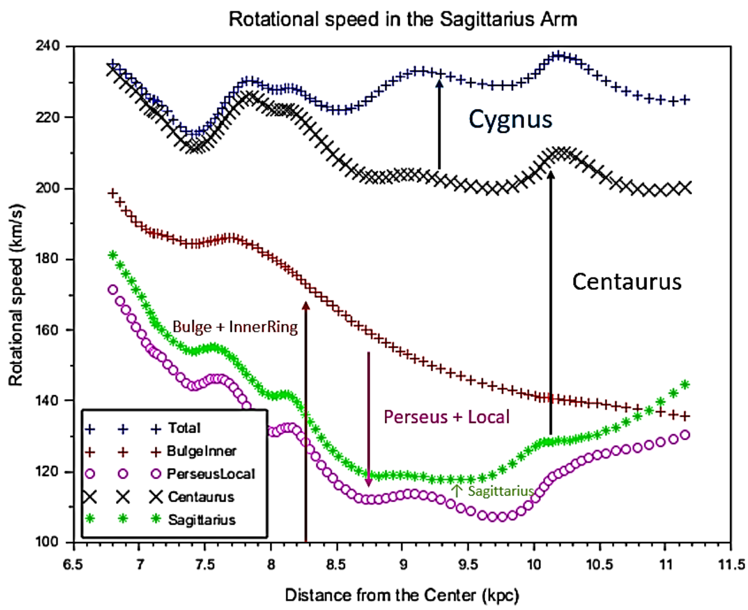

Figure 24. Sagittarius arm circular velocities.

Again, this positive impact of the Cygnus Arm is explained in **Figure 25** by the location of the start of the arm.

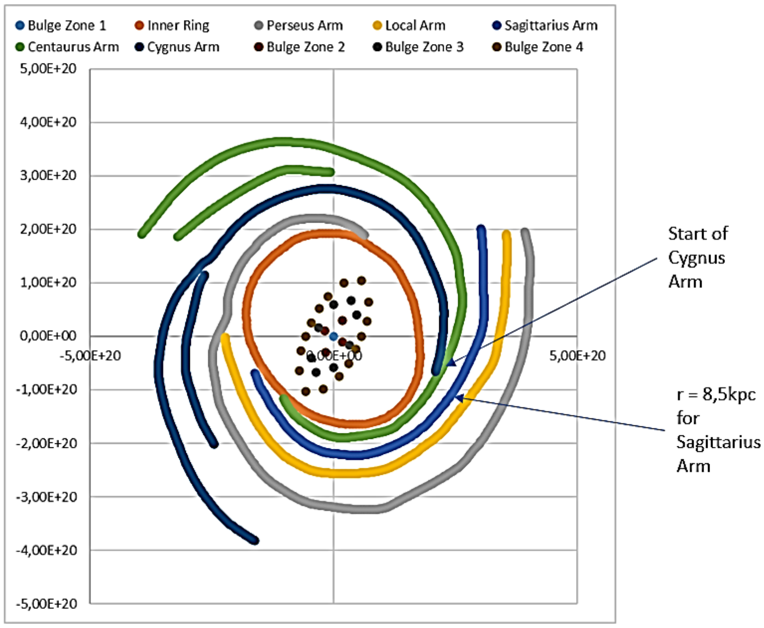

Figure 25. Cygnus and Sagittarius arms location.

For the Centaurus Arm, the situation is less easy to analyze. The positive contribution of the Cygnus Arm (the inner arm) is clearly visible for $r > 8.5$ kpc. For 7 kpc $< r < 8.5$ kpc, the results are not considered, as we are in a "junction area" (junction between Cygnus and Centaurus Arms, indicated by the gray area in Figure 26). For the area $r < 7$ kpc, the main contributors to radial acceleration and circular velocity are the Bulge and Inner Ring, while the rest of the Galaxy tends to decelerate the Centaurus Arm:

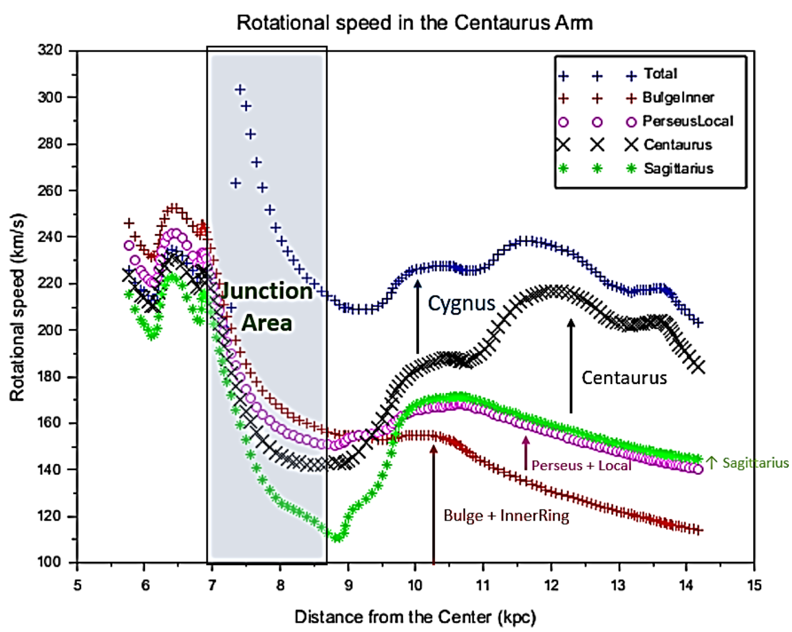

Figure 26. Centaurus arm circular velocities.

We can also see that the Sagittarius contribution to radial acceleration starts to be positive for $r > 10$ kpc, which corresponds to the tail location of the Sagittarius Arm, as shown in **Figure 27**.

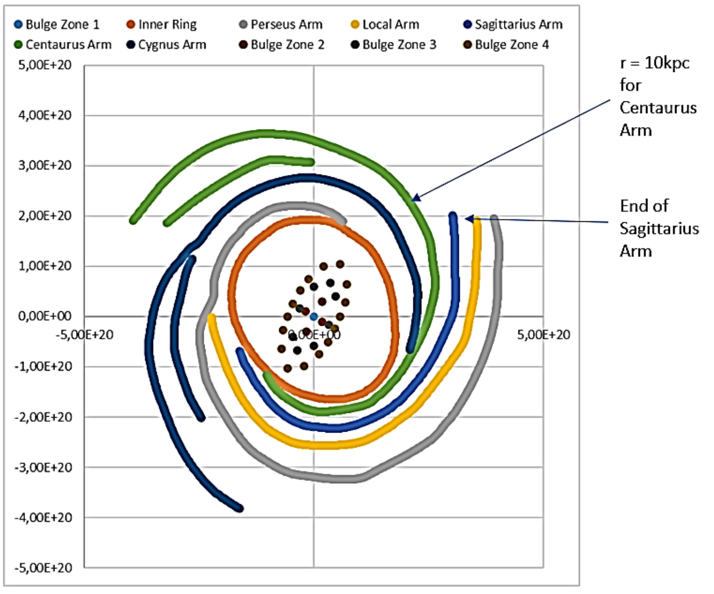

Figure 27. Centaurus and sagittarius arms location.

At last, for the Cygnus Arm, for $r > 12$ kpc we can see in **Figure 28** that the Cygnus contribution to itself drops:

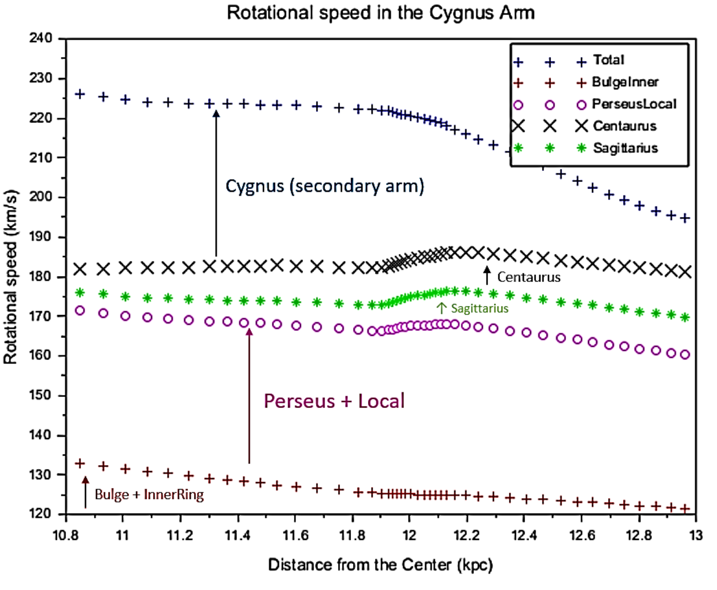

Figure 28. Cygnus Arm circular velocities.

In fact, this is where the "secondary Cygnus Arm" is ending as shown in **Figure 29**:

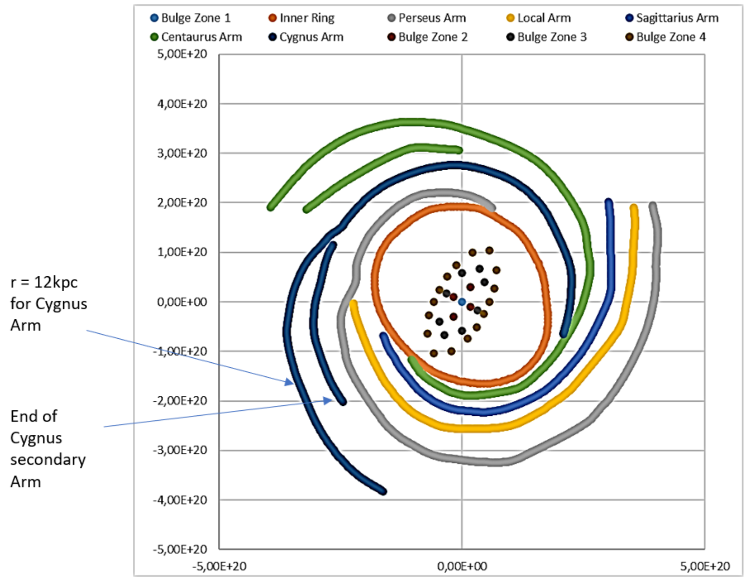

Figure 29. Cygnus arm location.

5. Conclusions

In this paper, we have tried to see the effect of each arm of the Milky Way on the global rotation movement, without using Dark Matter "disc model".

As we know, there are a lot of inconsistencies with the DM model (explained in § 2.2), and we see in our results that there are many logical explanations for the flatness of the rotation curves if we consider the global shape of our Galaxy.

Of course, there are uncertainties (detailed in §2.10), but the curve trends show that the inner arm always helps with the rotation motion, while the outer arm decelerates this motion.

As the "outer" arm is always "lighter" than the inner arm (because of the surface density profile, see Figure 6), the inner arm will always accelerate more than the outer arm decelerates.

In this way, the arms are carrying the impact of the gravitational forces from the Bulge to the tips of the arms.

6. Outlook

By using an iterative method, we have conducted dozens of simulations before reaching the optimal mass distribution that allows us to obtain similar results to the Gaia data.

Following this study, the total mass of our Galaxy for $r < 15$ kpc is not above 95.9 $\times 10^9$ M⊙.

Thus, the total mass of our Galaxy should not exceed $95.9 + 25 = 120.9 \times 10^9$ M⊙.

This estimation is 41% below the last lowest estimation of the Milky Way total mass with DM (estimated at 206×10^9 M⊙ in Jiao's paper [5]).

More globally, axisymmetric model needs around 40% more mass than non-axisymmetric model using the same data (see §4.1).

This method and model could be a possible explanation for the flatness of the Rotational Curve.

Conflicts of Interest

The author has no competing interests to declare that are relevant to the content of this article.

References

[1] Fux, R., Martinet, L. and Pfenniger, D. (1996) 3D N-Body Simulations of the Milky Way. In: Blitz, L. and Teuben, P., Eds., *Unsolved Problems of the Milky Way*, Springer, 125-131. https://doi.org/10.1007/978-94-009-1687-6_16

[2] Conselice, C.J., Wilkinson, A., Duncan, K. and Mortlock, A. (2016) The Evolution of Galaxy Number Density at z < 8 and Its Implications. *The Astrophysical Journal*, **830**, Article 83. https://doi.org/10.3847/0004-637x/830/2/83

[3] Loveday, J. (1996) The APM Bright Galaxy Catalogue. *Monthly Notices of the Royal Astronomical Society*, **278**, 1025-1048. https://doi.org/10.1093/mnras/278.4.1025

[4] Rubin, V.C., Thonnard, N. and Ford Jr., W.K. (1978) Extended Rotation Curves of High-Luminosity Spiral Galaxies. IV—Systematic Dynamical Properties, SA through Sc. *The Astrophysical Journal*, **225**, L107. https://doi.org/10.1086/182804

[5] Jiao, Y., Hammer, F., Wang, H., Wang, J., Amram, P., Chemin, L., *et al.* (2023) Detection of the Keplerian Decline in the Milky Way Rotation Curve. *Astronomy & Astrophysics*, **678**, A208. https://doi.org/10.1051/0004-6361/202347513

[6] Milgrom, M. (1983) A Modification of the Newtonian Dynamics as a Possible Alternative to the Hidden Mass Hypothesis. *The Astrophysical Journal*, **270**, 365-370. https://doi.org/10.1086/161130

[7] Kroupa, P., Pawlowski, M. and Milgrom, M. (2012) The Failures of the Standard Model of Cosmology Require a New Paradigm. *International Journal of Modern Physics D*, **21**, Article ID: 1230003. https://doi.org/10.1142/s0218271812300030

[8] Famaey, B. and McGaugh, S.S. (2012) Modified Newtonian Dynamics (MOND): Observational Phenomenology and Relativistic Extensions. *Living Reviews in Relativity*, **15**, Article No. 10. https://doi.org/10.12942/lrr-2012-10

[9] Feng, J.Q. (2020) Rotating Disk Galaxies without Dark Matter Based on Scientific Reasoning. *Galaxies*, **8**, Article 9. https://doi.org/10.3390/galaxies8010009

[10] Feng, J.Q. and Gallo, C.F. (2015) Deficient Reasoning for Dark Matter in Galaxies. *Physics International*, **6**, 11-22. https://doi.org/10.3844/pisp.2015.11.22

[11] Feng, J. and Gallo, C. (2014) Mass Distribution in Rotating Thin-Disk Galaxies According to Newtonian Dynamics. *Galaxies*, **2**, 199-222. https://doi.org/10.3390/galaxies2020199

[12] Feng, J.Q. and Gallo, C.F. (2011) Modeling the Newtonian Dynamics for Rotation Curve Analysis of Thin-Disk Galaxies. *Research in Astronomy and Astrophysics*, **11**, 1429-1448. https://doi.org/10.1088/1674-4527/11/12/005

[13] Marmet, L. (2012) Rotation Dynamics of a Galaxy with a Double Mass Distribution. arXiv: 1210.1998. http://arxiv.org/abs/1210.1998

[14] Ghosh, A., Rai, S. and Gupta, A. (1988) A Possible Servomechanism for Matter Distribution Yielding Flat Rotation Curves in Spiral Galaxies. *Astrophysics and Space Science*, **141**, 1-7. https://doi.org/10.1007/bf00641910

[15] Coquery, E. and Blanchard, A. (2025) Cosmological Implications of the *GAIA* Milky Way Declining Rotation Curve. *Astronomy & Astrophysics*, **703**, A88. https://doi.org/10.1051/0004-6361/202556337

[16] Portail, M., Gerhard, O., Wegg, C. and Ness, M. (2016) Dynamical Modelling of the Galactic Bulge and Bar: The Milky Way's Pattern Speed, Stellar and Dark Matter Mass Distribution. *Monthly Notices of the Royal Astronomical Society*, **465**, 1621-1644. https://doi.org/10.1093/mnras/stw2819

[17] Abuter, R., Amorim, A., Bauböck, M., Berger, J.P., Bonnet, H., Brandner, W., *et al.* (2019) A Geometric Distance Measurement to the Galactic Center Black Hole with 0.3% Uncertainty. *Astronomy & Astrophysics*, **625**, L10. https://doi.org/10.1051/0004-6361/201935656

[18] Maíz-Apellániz, J. (2001) The Spatial Distribution of O–B5 Stars in the Solar Neighborhood as Measured by *Hipparcos*. *The Astronomical Journal*, **121**, 2737-2742. https://doi.org/10.1086/320399

[19] Prša, A., Harmanec, P., Torres, G., Mamajek, E., Asplund, M., Capitaine, N., *et al.* (2016) Nominal Values for Selected Solar and Planetary Quantities: IAU 2015 Resolution B3. *The Astronomical Journal*, **152**, Article 41. https://doi.org/10.3847/0004-6256/152/2/41

[20] Borrero, Z., *et al.* (2005) Earth Science: Geology, the Environment, and the Universe. The McGraw-Hill Companies, Inc.

[21] Li, X., Yang, P., Wang, H., Li, Q., Luo, Y., Luo, Z., *et al.* (2024) Asymmetric Drift Map of the Milky Way Disk Populations between 8-16 kpc with LAMOST and Gaia Datasets. *The Open Journal of Astrophysics*, **7**. https://doi.org/10.33232/001c.117594

[22] Dehnen, W., McLaughlin, D.E. and Sachania, J. (2006) The Velocity Dispersion and Mass Profile of the Milky Way. *Monthly Notices of the Royal Astronomical Society*, **369**, 1688-1692. https://doi.org/10.1111/j.1365-2966.2006.10404.x

[23] Khoperskov, S., Gerhard, O., Di Matteo, P., Haywood, M., Katz, D., Khrapov, S., *et al.* (2020) Hic Sunt Dracones: Cartography of the Milky Way Spiral Arms and Bar Resonances with *GAIA* Data Release 2. *Astronomy & Astrophysics*, **634**, L8. https://doi.org/10.1051/0004-6361/201936645

[24] Bovy, J. and Rix, H. (2013) A Direct Dynamical Measurement of the Milky Way's Disk Surface Density Profile, Disk Scale Length, and Dark Matter Profile at 4 kpc $\lesssim R \lesssim$ 9 kpc. *The Astrophysical Journal*, **779**, Article 115. https://doi.org/10.1088/0004-637x/779/2/115

[25] Miyamoto, M. and Nagai, R. (1975) Three-Dimensional Models for the Distribution of Mass in Galaxies. *Publications of the Astronomical Society of Japan*, **27**, 533-543. https://doi.org/10.1093/pasj/27.4.533

[26] Athanassoula, E. (2005) On the Nature of Bulges in General and of Box/Peanut Bulges in Particular: Input from *N*-Body Simulations. *Monthly Notices of the Royal Astronomical Society*, **358**, 1477-1488. https://doi.org/10.1111/j.1365-2966.2005.08872.x

[27] Liang, Z.Z., Wang, J., Gao, H., Ho, L.C. and Athanassoula, E. (2025) Connection between Nonaxisymmetric Structures and Neutral Gas Distribution in Disk Galaxies. *The Astrophysical Journal*, **983**, Article 61. https://doi.org/10.3847/1538-4357/ad87f1

Appendix

Appendix 1

For the mass distribution in the spiral area, we have started using a power law with a power of $\alpha = -2.25$ with this mass distribution, summarized in Table A1:

Table A1. Power law mass distribution in the spiral area.

Area (kpc)	$4.2 < r < 5$	$5 < r < 6$	$6 < r < 6.8$	$6.8 < r < 8$	$8 < r < 9$	$9 < r < 11$	$11 < r < 13$	$13 < r < 15$
Mass (*10^9 M⊙)	11.7	12.0	8.0	10.1	7.0	11.4	9.0	7.2

After iterations, we arrive at this mass distribution, summarized in Table A2:

Table A2. Simulation mass distribution in the spiral area.

Area (kpc)	$4.2 < r < 5$	$5 < r < 6$	$6 < r < 6.8$	$6.8 < r < 8$	$8 < r < 9$	$9 < r < 11$	$11 < r < 13$	$13 < r < 15$
Mass (*10^9 M⊙)	9.4	9.4	7.3	15.0	9.3	14.9	7.3	3.8

This important change, especially for 6.8 kpc < r < 11 kpc area, could be explained by a growth factor linked to the arm's width (if the mass density is spread equally in the arm's width, then the bodies' location of inner arm is less beneficial to increase the rotation of outer arm).

If we consider all the arms with a width e and with also inter-arm distance equal to e, the best-case scenario would be to have half the mass of inner arm at $e - \frac{e}{4}$ and the other half at $e + \frac{e}{4}$.

Then the new radial acceleration contribution from inner arm to outer arm will be:

$$a_{new} = \frac{Gm}{2} * \left(\frac{1}{\left(e - \frac{e}{4}\right)^2} + \frac{1}{\left(e + \frac{e}{4}\right)^2} \right) = \frac{Gm}{2e^2} \left(\frac{1}{\left(\frac{3}{4}\right)^2} + \frac{1}{\left(\frac{5}{4}\right)^2} \right)$$

$$= \frac{Gm}{2e^2} * \left(\frac{16}{9} + \frac{16}{25} \right) = \frac{Gm}{e^2} * \left(\frac{8}{9} + \frac{8}{25} \right) = a_{old} * \left(\frac{8}{9} + \frac{8}{25} \right)$$

It means the grow factor on spiral masses could be up to 1.21 ($\approx \frac{8}{9} + \frac{8}{25}$).

Even with this growth factor, the mass distribution does not fit with our power law for 6.8 kpc < r < 11 kpc area, and does not allow us to fully use the Baryonic mass Surface density profile.

Appendix 2

For the determination of Inner Ring mass, we have taken into account the spiral mass for r < 6.8 kpc (equal to 5.1 × 10^9 M⊙, see Table 1) and deduced it from the total mass between 4.2 and 6.8 kpc (9.4 + 9.4 + 7.3 = 26.1, see Table A2), then we obtain an Inner Ring mass equal to 21 × 10^9 M⊙.

Appendix 3

For the determination of the mass of the Galaxy for $r > 15$ kpc, we keep the same power law (Equation (2)), integrated between $r = 15$ kpc and $r = 26.5$ kpc.

This mass $m_{15\text{ to }26.5}$ is defined as (integration of Equation (2) between 15 and 26.5 kpc):

$$\begin{aligned} m_{15\text{ to }26.5} = &\left(\left(\left((-1.81818)*(1+26.5\text{ kpc})^{-0.55}\right)+0.64516*(1+26.5\text{ kpc})^{-1.55}\right)\right. \\ &\left.-\left(\left((-1.81818)*(1+15\text{ kpc})^{-0.55}\right)+0.64516*(1+15\text{ kpc})^{-1.55}\right)\right)*2*\rho_0*\pi \\ &\approx 25\times 10^9 M_\odot \end{aligned}$$